

LIDAR Sensing for Vehicle Lateral Guidance: Algorithm and Experimental Study

Guang Lu, *Member, IEEE*, and Masayoshi Tomizuka, *Fellow, IEEE*

Abstract—This paper describes a new vehicle detection system based on a laser imaging, detection, and ranging (LIDAR) sensor, and conducts an experimental study to investigate the sensor's role in the current California PATH vehicle lateral guidance systems. The LIDAR sensor is installed on a controlled vehicle and it can measure the relative distance of the vehicle from a preceding vehicle, by scanning the horizontal plane with laser beams. Environmental clutter becomes the main challenge in data processing, when LIDAR tries to track the desired target. A probabilistic data association-based algorithm has been developed to solve this problem, which has been verified in real-time experiments using two Buick LaSabre vehicles. The experimental study also reveals the relation between the LIDAR outputs and the magnetic reference system widely used by the current PATH lateral control systems, and the results provide the guidelines on how this new sensor system may be used for vehicle lateral guidance.

Index Terms—Automated highways, laser scanning radar, vehicle following, vehicle lateral guidance.

I. INTRODUCTION

IN AN automated highway system (AHS), each vehicle is automatically controlled in both longitudinal and lateral directions, and the intervehicle distance is kept small within each platoon so that the highway capacity can be increased by 2–6 times over current peak capacities [1], [2]. Lane keeping, i.e., regulation of lateral deviation from the road centerline becomes the goal of any vehicle lateral control system. This has placed sensing technology on a critical role, as the lateral control system relies on the onboard sensors to detect the lateral deviation of the vehicle. Magnetometers [3]–[5], vision systems [6]–[9], and GPS [7] have been so far proposed to achieve this goal. However, all these sensing schemes require some kind of road infrastructure. Magnetometers can only detect distance from magnets, and hence magnets need to be buried under the road centerline for possible lateral guidance. Vision systems require clear lane markers, and GPS beacons are often required to make the GPS measurement possible.

The requirement of road infrastructure can be removed, if another vehicle is used as a lead vehicle to laterally guide the controlled one along the road centerline. This is called autonomous vehicle following (AVF) control [10]–[12]. The AVF allows a vehicle to be automatically controlled to follow its preceding vehicle to achieve the lane-keeping performance. The main benefit

of this approach is that it requires no road infrastructure, as it only needs an onboard sensor to detect the relative distance between the two vehicles. Thus, technically, autonomous lateral following is much easier to realize, although it requires the lead vehicle, which may be manually controlled, to follow the road reasonably well.

A key technical challenge in AVF is the detection of the relative intervehicle distance, especially the lateral distance. This is how a new laser imaging, detection, and ranging (LIDAR) sensor was introduced to the California (partners for advanced transit and highways) PATH lateral guidance system. LIDAR scans in the horizontal plane at every sampling step, and may detect the position of any reflective target. However, clutter in the environment causes severe challenges in LIDAR sensing as the sensor tries to track the desired target, i.e., the leading vehicle.

It is an interesting question as to how the new LIDAR sensor fits into the current lateral guidance systems. Most of the current PATH lateral controllers rely on the use of two sets of magnetometers, one mounted under the front bumper and the other mounted under the rear bumper, for detection of the vehicle lateral deviation. Understanding the relation between the LIDAR and the magnetometers may help to create a better sensor management system for enhanced vehicle and passenger safety through fault-detection and fault-tolerant algorithms. Such a discovery may also lead to similar improvements in other types of vehicle lateral guidance systems, e.g., vision or GPS systems.

This paper presents a probabilistic-data-association-based data processing algorithm for LIDAR to accurately track the preceding vehicle, in spite of the environmental clutter. This algorithm is verified in real-time experiments involving a platoon of two Buick vehicles. An experimental study is also conducted to investigate the relation between the LIDAR and the magnetometer measurements.

The rest of the paper is organized as follows. Section II describes the working scheme of the LIDAR sensor being used. Section III briefly introduces the data processing algorithms for LIDAR sensor. This is followed by a detailed derivation in Section IV. Experimental validation is presented in Section V. An experimental study is then conducted to investigate the relation between the LIDAR and the magnetometer measurements in Section VI. Finally, Section VII concludes this paper.

II. LASER SCANNING RADAR SENSOR

A LIDAR sensor shown in Figs. 1 and 2 has been used to measure the relative distance from the leading vehicle to the following vehicle. As shown in Fig. 3, the LIDAR sensor consists of a laser diode, a scanning mechanism, and a receiver. The laser

Manuscript received July 10, 2005; revised May 30, 2006. Recommended by Technical Editor H. Hashimoto. This work was supported by the California Department of Transportation (CalTrans) under PATH TO4204.

G. Lu is with the Department of Mechanical Engineering, Tulane University, New Orleans, LA 70118 USA (e-mail: glu1@tulane.edu).

M. Tomizuka is with the Department of Mechanical Engineering, University of California, Berkeley, CA 94720 USA (e-mail: tomizuka@me.berkeley.edu).
Digital Object Identifier 10.1109/TMECH.2006.886192



Fig. 1. LIDAR mounted on top of the vehicle.



Fig. 2. LIDAR: A closer look.

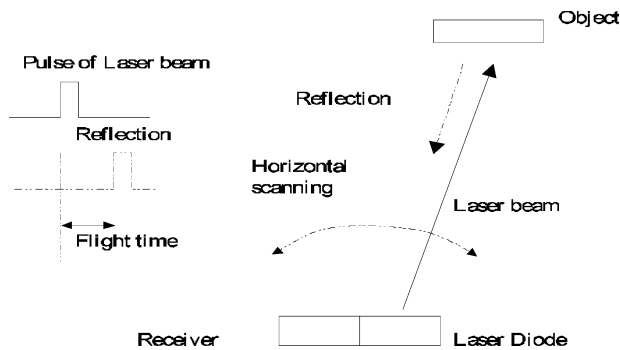


Fig. 3. LIDAR working scheme.

diode emits laser beams to the roadway. The scanning mechanism is a rotating prism, and it makes the laser beams scan in the horizontal plane. If the laser beams hit any reflective object on the roadway, they will bounce back. The reflected laser beams can be detected by the built-in receiver. The distance from the sensor to the object is measured by the “Time of Flight” (TOF) principle, which says

$$s = cT \quad (1)$$

where s is the distance from the sensor to the target, T is the flight time of the laser beam before it reaches the target, and c is the speed of light, which is 2.976×10^8 m/s. Since the laser beams scan in the horizontal plane with constant steps, the orientation of the object can also be measured by counting the number of the scanning steps. Hence, the position of an object is uniquely defined in a two-dimensional (2-D) space. The measured position is written in polar coordinates, and can be later converted to Cartesian coordinates. In this research, a target with a reflective surface is fixed on the rear bumper of the leading vehicle, and a LIDAR sensor is installed on the

TABLE I
LIDAR SPECIFICATION

class of laser beam	class 1
wave length	800 nm (infrared)
maximum measurable distance	153 m
distance resolution	0.15 m
number of scanning steps	80
scanning angle of each step	0.15°
scanning range of angle	12°
vertical beam width	4°

TABLE II
DATA SPECIFICATION FOR LIDAR

Serial Communication Specification	Value
speed	38400 bps
start bit	1 bit
data length	8 bits
parity	Even
stop bit	1 bit

following vehicle. Therefore, the relative distance between the two test vehicles can be measured in real time.

The laser beam emitted by the LIDAR sensor used in this study scans horizontally 12° in 80 equal steps for every 100 ms. At each step, the LIDAR sensor measures the distance and angular position of the object that reflects the laser beams along with the intensity of the reflection. The intensity information is shown in the form of an integer varying from 0 to 31. The specification of the LIDAR sensor is shown in Table I. For example, if the longitudinal distance between the two vehicles is 10 m, the width of the scanning area is about 2 m with the resolution of 0.025 m. A set of 162-byte data is transmitted every 100 ms cycle through the serial port. The data specification is listed in Table II.

III. PROBABILISTIC DATA ASSOCIATION

When the laser beam scans, it detects anything reflective on the roadway. Since there are numerous reflective objects and surfaces in the environment, the LIDAR sensor returns one set of measurements in every scanning step. For each sampling period, the LIDAR sensor returns 80 sets of measurements, most of which are not related to the desired target. Extraction of the useful information about the real position of the desired target from the sensor measurements has thus become a key research issue.

At the first thought, picking one measurement that has the strongest intensity value seems to be a natural idea. However, two main concerns arise about this method. First, the intensity data is quite rough, because it is an integer varying from 0 to 31. Hence it is not practical to rely on the intensity data to make the decision. Second, picking only one measurement is of high risk, because the algorithm is very likely to keep tracking a wrong target if a wrong selection has been made at some sampling point in the past.

To determine the actual position of the target of interest, a probability data association method proposed by Bar-Shalom and Tse [13] has been applied to process the LIDAR measurements. The fundamental idea of the data processing algorithm is to combine all the validated measured data, according

to their probabilities of being the correct measurement to update a Kalman filter. The data points that are more likely to be the correct measurements receive higher weights in the algorithm than other data points. This is mainly based on the *a priori* assumption that all measurements are normally distributed around a predicted point.

Details of this algorithm are described in Section IV.

IV. LIDAR DATA PROCESSING ALGORITHM

The dynamics of the target in track, i.e., the lead vehicle, are modeled by the following equation:

$$x[k+1] = Fx[k] + Gn[k] \quad (2)$$

where $x[k]$ is the state vector consisting of the position and velocity of the lead vehicle relative to the following vehicle in Cartesian coordinates

$$x[k] = [x_r \ \dot{x}_r \ y_r \ \dot{y}_r]^T \quad (3)$$

and $n[k]$ consists of the relative acceleration in x and y directions

$$n[k] = \begin{pmatrix} \ddot{x}_r[k] \\ \ddot{y}_r[k] \end{pmatrix}. \quad (4)$$

In vehicle following testing, the relative acceleration should be kept small, and we further assume $n[k]$ to be normally distributed, zero mean, white process noise, with the variance

$$E(n[k]n^T[j]) = N[k]\delta_{kj}. \quad (5)$$

In practice, $N[k]$ may be chosen as a diagonal constant matrix.

Then, F and G are constant matrices and can be calculated as follows.

$$F = \begin{pmatrix} 1 & T_s & 0 & 0 \\ 0 & 1 & 0 & 0 \\ 0 & 0 & 1 & T_s \\ 0 & 0 & 0 & 1 \end{pmatrix} \quad (6)$$

$$G = \begin{pmatrix} T_s^2/2 & 0 \\ T_s & 0 \\ 0 & T_s^2/2 \\ 0 & T_s \end{pmatrix} \quad (7)$$

where T_s is the sampling time of LIDAR sensor.

Remark on the Sampling Time: The value of the sampling time decides the accuracy of the one-step prediction in the algorithm. Hence, smaller sampling time usually leads to better performance. However, the selection of the sampling time is subject to the physical limitations posed by the sensor, i.e., how fast the LIDAR can scan, since the estimation algorithm has to rely on the real-time measurements as feedback information. In this case, the sensor specification determines that $T_s = 100$ ms. For vehicle guidance system to work, a sampling frequency of at least 10 Hz is usually necessary. It should also be noted that smaller sampling time also increases the computation load, which may cause failure of the system, especially when large amount of measurements have to be processed in real time.

Although LIDAR measurements arrive in polar coordinates, they are converted to Cartesian. Accordingly, the measurement model for one measurement is given by

$$z[k] = Hx[k] + v[k] \quad (8)$$

where

$$H = \begin{pmatrix} 1 & 0 & 0 & 0 \\ 0 & 0 & 1 & 0 \end{pmatrix} \quad (9)$$

and $v[k]$ consists of the zero mean, white process noise, and Gaussian measurement noises in x and y directions as

$$v[k] = \begin{pmatrix} v_x[k] \\ v_y[k] \end{pmatrix} \quad (10)$$

with the variance

$$E(v[k]v^T[j]) = R[k]\delta_{kj}. \quad (11)$$

In the last equation, $R[k]$ is the measurement noise covariance at time index k , which can be converted from the measurement noise variance in polar coordinates according to Li and Bar-Shalom [14]

$$R[k] \approx \frac{\sigma_r^2 - r^2\sigma_\theta^2}{2} \begin{bmatrix} b + \cos(2\theta) & \sin(2\theta) \\ \sin(2\theta) & b - \cos(2\theta) \end{bmatrix} \quad (12)$$

where

$$b = \frac{\sigma_r^2 + r^2\sigma_\theta^2}{\sigma_r^2 - r^2\sigma_\theta^2} \quad (13)$$

and σ_r and σ_θ are the standard deviations of the associated polar coordinate measurement noise. $x[0]$, $n[k]$, and $v[k]$ are assumed to be independent.

Remark on the Selection of σ_r and σ_θ : Smaller values for σ_r and σ_θ result in a stronger feedback gain in the estimation, which may achieve better performance when the measurements are associated with little noise. However, when the measurements are noisy, the algorithm may not converge. The values of σ_r and σ_θ may be selected according to the specifications of the sensor, i.e., resolution of the distance and angle measurements. In this paper, $\sigma_r = 0.3$ m and $\sigma_\theta = 0.0026$ rad (0.15°).

However, LIDAR returns more than just one measurement at each sampling time step. At time index k , there are 80 measurements, denoted by $\{z_i[k]\}_{i=1}^{80}$. Assume that some kind of validation test is conducted, which will be described later, so that only $m[k]$ ($m[k] \leq 80$) measurements are considered as candidates for a correct return. Denote the set of validated measurements at time k as

$$Z[k] = \{z_i[k]\}_{i=1, \dots, m[k]} \quad (14)$$

and the set containing all the previous validated measurements up to time index k as

$$Z^k = \{Z[j]\}_{j=1, \dots, k}. \quad (15)$$

Now, the problem is how to obtain the optimal estimate of the state vector based on all the past measurements, i.e., $E\{x[k]|Z^k\}$.

Based on the past observations, the algorithm predicts the state of the target for the current time step. The prediction equations are

$$\hat{x}[k|k-1] = F\hat{x}[k-1|k-1] \quad (16)$$

$$\hat{z}[k|k-1] = H\hat{x}[k|k-1]. \quad (17)$$

If only a single measurement at the k th step, e.g., $z_i[k]$, is chosen for the estimation as if it is known as a correct return, a standard Kalman filter provides

$$\hat{x}_i[k|k] = \hat{x}[k|k-1] + W[k]v_i[k] \quad (18)$$

$$W[k] = P[k|k-1]H^T(HP[k|k-1]H^T + R[k])^{-1} \quad (19)$$

where

$$v_i[k] = z_i[k] - \hat{z}[k|k-1] \quad (20)$$

and $P[k|k-1]$ represents the state estimation covariance.

In probabilistic data association, instead of picking only one measurement, all the validated measurements will be combined probabilistically. Define the following events as

$$\begin{aligned} \chi_i[k] &= \{z_i[k] \text{ is the correct measurement}\} \\ i &= 1, \dots, [k] \end{aligned} \quad (21)$$

$$\chi_0[k] = \{\text{none of the validated measurements is correct}\}. \quad (22)$$

Assuming that only one return can be correct at any time index, the above events are mutually exclusive and exhaustive. Then, the desired optimal estimate of the state vector can be calculated as

$$\begin{aligned} \hat{x}[k|k] &= E\{x[k]|Z^k\} \\ &= \sum_{i=0}^{m[k]} E\{x[k]|\chi_i[k], Z^k\} P\{\chi_i[k]|Z^k\} \\ &= \sum_{i=0}^{m[k]} \hat{x}_i[k|k] P\{\chi_i[k]|Z^k\}. \end{aligned} \quad (23)$$

Define

$$\beta_i[k] = P\{\chi_i[k]|Z^k\} \quad (24)$$

to be the probabilistic weight according to which all the candidate measurements should be combined in the estimation. Note that this is a *posteriori* probability. It is assumed that no inference can be made on the number or distribution of incorrect returns from the past measurements. However, the algorithm assumes the *a priori* probability density of a correct measurement, conditioned upon all the past measurements to be normal, with mean $\hat{z}[k|k-1]$ and covariance $S[k]$. Such a probability density function is then truncated to fit in the validation region, which is the set containing all the validated measurements. Hence

$$p(z_i[k]|\chi_i[k], Z^{k-1}, m[k]) = \frac{e^{-(1/2)v_i^T[k]S^{-1}[k]v_i[k]}}{2(1-\alpha_1)\pi\sqrt{|S[k]|}} \quad (25)$$

where α_1 is the preselected probability that the correct return is not included in the validation region, and

$$S[k] = HP[k|k-1]H^T + R[k] \quad (26)$$

is the measurement covariance.

Now, $\beta_i[k]$ can be calculated according to Bayes' rule

$$\begin{aligned} \beta_i[k] &= P\{\chi_i[k]|Z^k, m[k]\} \\ &= c_k^{-1} p(Z_k|\chi_i[k], Z^{k-1}, m[k]) \\ &\quad \times P\{m[k]|\chi_i[k], Z^{k-1}\} P\{\chi_i[k]|Z^{k-1}\} \end{aligned} \quad (27)$$

where

$$\begin{aligned} c_k &= \sum_{i=0}^{m[k]} p(Z_k|\chi_i[k], Z^{k-1}, m[k]) \\ &\quad \times P\{m[k]|\chi_i[k], Z^{k-1}\} P\{\chi_i[k]|Z^{k-1}\}. \end{aligned} \quad (28)$$

Calculation of each term in the above equations is described as follows.

Let $I[k]$ denote the number of incorrect returns at the time index k . Due to the assumption that there is only one correct return at index k , the value of $I[k]$ can only be equal to $m[k]$, i.e., the correct return does not fall in the validation region, or $m[k]-1$, i.e., the correct return falls in the validation region. Hence

$$P\{m[k]|\chi_i[k], Z^{k-1}\} = P\{I[k] = m[k]-1|Z^{k-1}\} \quad \text{for } i \neq 0 \quad (29)$$

and

$$P\{m[k]|\chi_0[k], Z^{k-1}\} = P\{I[k] = m[k]|Z^{k-1}\}. \quad (30)$$

Because of the assumption that no inference can be made on the number of incorrect returns from past data, the above two probabilities are assumed equal. Thus, the term $P\{m[k]|\chi_i[k], Z^{k-1}\}$ in the numerator of (27) can be cancelled out by the same term in the denominator, i.e., (28).

It is also assumed that $P\{\chi_i[k]|Z^{k-1}\}$ is the same for all $i \neq 0$. Let α_2 be the probability for the case that the correct target position is not detected by the LIDAR sensor, i.e., it is not shown in any measurement. Then, by incorporating the intensity data generated by LIDAR $\phi_i[k]$, we may get

$$P\{\chi_i[k]|Z^{k-1}\} = \frac{\phi_i[k](1-\alpha_1)(1-\alpha_2)}{\sum_{j=1}^{m[k]} \phi_j[k]}. \quad (31)$$

It is clear that

$$P\{\chi_0[k]|Z^{k-1}\} = \alpha_1 + (1-\alpha_1)\alpha_2. \quad (32)$$

To calculate $p(Z_k|\chi_i[k], Z^{k-1}, m[k])$, the algorithm assumes that all the incorrect measurements are uniformly distributed within the validation region, i.e., the probability for an incorrect measurement to appear in any place within the region is considered the same. Now, let the volume of the validation region at time index k be $V[k]$, which will be calculated later, then the uniform distribution assumption implies that the probability

density function for a single incorrect measurement is

$$p\{z_i[k]|z_i[k] \text{ is incorrect}\} = \frac{1}{V[k]}. \quad (33)$$

Hence, when there are $m[k]$ or $m[k] - 1$ independent incorrect measurements, the probability density function becomes either

$$p(Z_k|\chi_0[k], Z^{k-1}, m[k]) = V[k]^{-m[k]} \quad (34)$$

or

$$p(Z_k|\chi_i[k], Z^{k-1}, m[k]) = V[k]^{-(m[k]-1)} \\ \times p(z_i[k]|\chi_i[k], Z^{k-1}, m[k]) \quad \text{for } i \neq 0. \quad (35)$$

After some calculations,

$$\beta_0[k] = \frac{\psi \sum_{i=1}^{m[k]} \phi_i[k]}{V[k](1-\alpha_2)\phi_i[k] + \sum_{j=1}^{m[k]} \left[\frac{e^{-(1/2)v_j^T[k]S^{-1}[k]v_j[k]} \phi_j[k]}{2\pi\sqrt{|S[k]|}} \phi_i[k] \right]}, \quad (36)$$

and

$$\beta_i[k] = \frac{e^{-(1/2)v_i^T[k]S^{-1}[k]v_i[k]}}{2\pi\sqrt{|S[k]|}} \\ \frac{\psi \sum_{i=1}^{m[k]} \phi_i[k]}{V[k](1-\alpha_2)\phi_i[k] + \sum_{j=1}^{m[k]} \left[\frac{e^{-1/2v_j^T[k]S^{-1}[k]v_j[k]} \phi_j[k]}{2\pi\sqrt{|S[k]|}} \phi_i[k] \right]} \\ \text{for } i = 1, \dots, m[k]. \quad (37)$$

where

$$\psi = \alpha_1 + \alpha_2 - \alpha_1\alpha_2. \quad (38)$$

The estimation is now updated by

$$\hat{x}[k|k] = \hat{x}[k|k-1] + W[k]v[k] \quad (39)$$

$$v[k] = \sum_{i=1}^{m[k]} v_i[k]\beta_i[k]. \quad (40)$$

It is clear from the above equations that all the validated measurements are combined according to their posterior probability of being the correct measurements and the weighted sum is used to update the estimation mechanism. Because of the way the probabilities are assigned, those measurements that are closer to the predicted point receive higher weights as they are more likely to be the correct measurements.

Remark on the Selection of α_1 and α_2 : α_1 is the probability that the target has been detected but the correct measurement has not been included in the validation region, and α_2 is the probability that the target is not detected. These values are both preselected and the selection of these parameters is according to the following considerations. It can be shown from (36) and (37) that $\beta_i[k]$ will decrease, when a larger value is chosen for either of these two parameters. This implies that when the uncertainty increases, the algorithm tends to reduce the weights on all the validated measurements. These two equations also show that the increase of α_2 has stronger effects on the probability weights than α_1 , which implies that missing the detection will be considered worse than not including the correct measurement

into the validation region. In this paper, the two parameters are chosen as $\alpha_1 = 0.02$ and $\alpha_2 = 0.05$.

The covariance of the estimation is given by

$$P[k|k] = \beta_0[k]P[k|k-1] + (1-\beta_0[k])(I-W[k]H)P[k|k-1] \\ + W[k] \left[\left(\sum_{i=1}^{m[k]} v_i[k]v_i^T[k]\beta_i[k] \right) - v[k]v^T[k] \right] W^T[k] \quad (41)$$

where the first two terms can be considered as the covariance as if there is only one return, and

$$P[k|k-1] = FP[k-1|k-1]F^T + GN[k-1]G^T. \quad (42)$$

Now the validation condition is introduced. All the validated measurements have to satisfy

$$v_i^T[k]S^{-1}[k]v_i[k] \leq \gamma. \quad (43)$$

The above condition is used to determine a neighborhood around the predicted point, since $v_i[k]$ is the deviation of the i th measurement from the predicted point at time index k . Since the LIDAR measurements are 2-D (in the horizontal plane), the bound γ is determined from χ -squared tables, with two degrees of freedom corresponding to the probability α_1 of rejecting the correct LIDAR measurements. Only the measurements which fall into this neighborhood are used to update the estimation. It is clear that the validation region increases with both γ and the measurement noise covariance $S[k]$. When uncertainty increases in the measurements, i.e., $S[k]$ becomes larger, the validation region increases to include more candidate measurements.

The volume of the validation region is

$$V[k] = \pi\gamma|S[k]|^{1/2}. \quad (44)$$

For the 2-D case, this is the area of an ellipse.

V. EXPERIMENTAL RESULT

Real-time experiments have been conducted using two Buick test vehicles on the test track at Richmond Field Station, University of California, Berkeley. The test track is used for low-speed vehicle testing, and it has an embedded magnetic reference system, i.e., equally spaced magnets are buried under the road centerline for magnetic detection. Each test vehicle is equipped with magnetometers to detect the vehicle's lateral deviation from the centerline. The track consists of many sharp curves, as shown in Fig. 4, which makes it challenging for even low-speed testing.

The vehicle with installed LIDAR was used as the following vehicle, and both vehicles were controlled to achieve lane-keeping performance. Intervehicle communication was used to record the real-time measurements of both vehicles simultaneously. The longitudinal distance between the two vehicles was manually controlled in the tests. Figs. 5 and 6 show the outputs from the LIDAR detection system after data processing. During testing, the two vehicles were driven up to around 9 m/s (about 20 mph), which was close to the speed limit allowed on the test track. Fig. 7 shows the wheel speed recorded for the two vehicles. Fig. 8 compares the relative wheel speed $v_{\text{lead}} - v_{\text{follower}}$

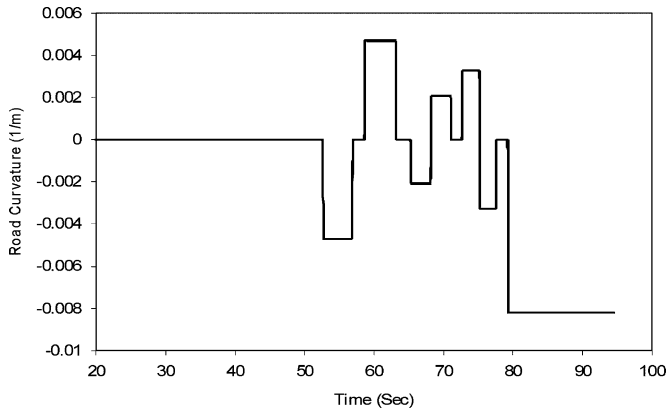


Fig. 4. Road curvature.

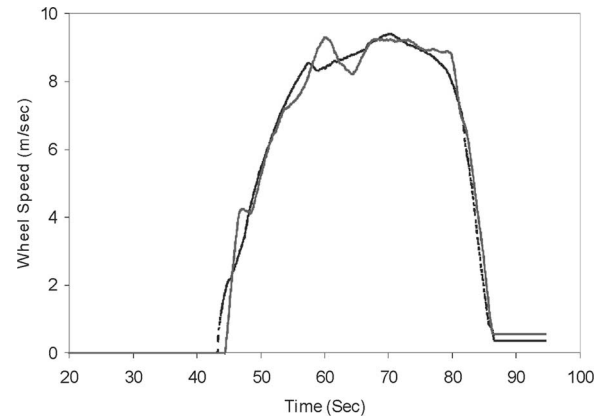


Fig. 7. Vehicle wheel speed. (Dotted line) Lead vehicle. (Solid line) Following vehicle.

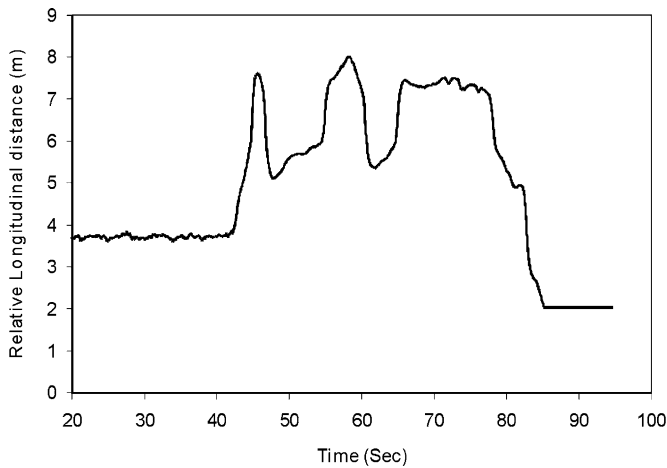


Fig. 5. Relative longitudinal distance between the two vehicles.

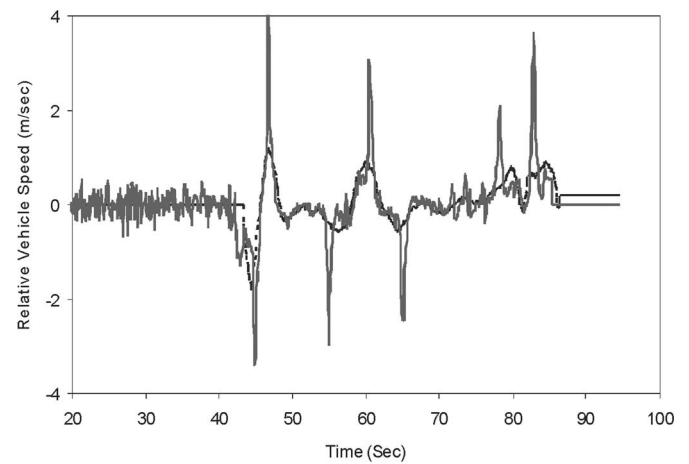


Fig. 8. Relative inter vehicle velocity. (Dotted line) Relative wheel speed. (Solid line) Estimated from LIDAR.

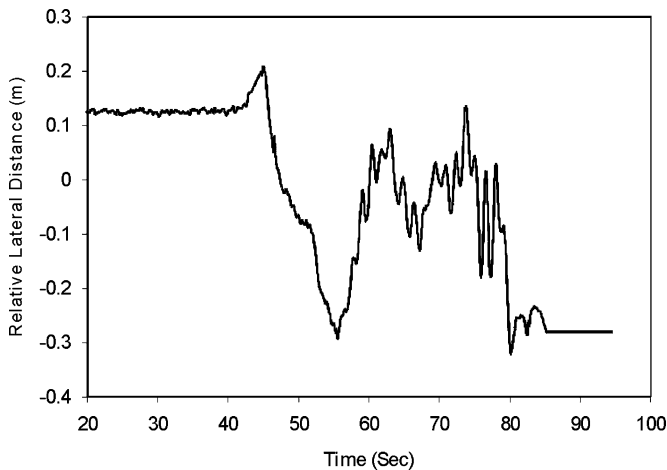


Fig. 6. Relative lateral distance between the two vehicles.

to the estimated relative velocity according to LIDAR measurements, which was calculated by

$$v_{rel}[k] = \frac{\sqrt{x_r^2[k] + y_r^2[k]} - \sqrt{x_r^2[k-1] + y_r^2[k-1]}}{T_s}. \quad (45)$$

It can be seen from the figure that the estimated relative velocity approximately matched the relative wheel speed recorded through the intervehicle communication. The two matched especially well when the relative velocity changed gradually, i.e., when the relative acceleration was small, as assumed in the kinematic model. Big spikes in the estimates appeared, whenever the actual relative velocity underwent abrupt changes. However, LIDAR did manage to track the target in spite of these spikes generated occasionally, thanks to the probabilistic data association.

VI. RELATION BETWEEN LIDAR AND MAGNETOMETERS

As a new sensor in the lateral guidance system developed by California PATH, LIDAR may work more efficiently if it could be integrated into the existing magnetometer-based sensing scheme. However, there is fundamental difference between LIDAR and magnetometer measurements in terms of lateral guidance. LIDAR measures the vehicle's relative distance from a preceding vehicle, which is presumed to be following the road centerline, while the magnetometers measure the vehicle's lateral deviation from the road centerline directly. Intuitively, if the preceding vehicle follows the road centerline sufficiently close,

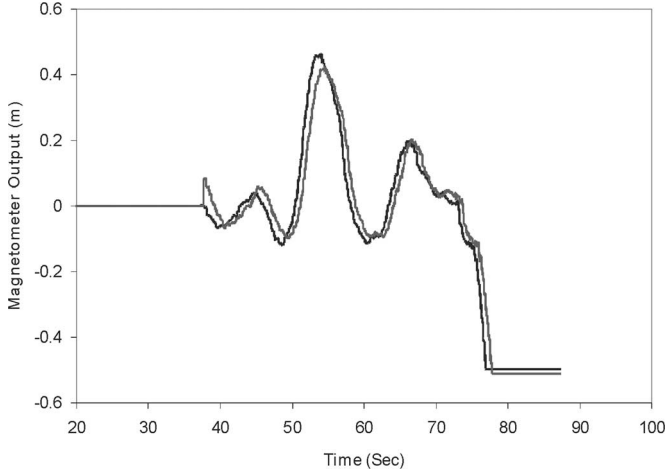


Fig. 9. Magnetometer outputs. (Dashed line) Rear magnetometer output. (Solid line) Front magnetometer output.

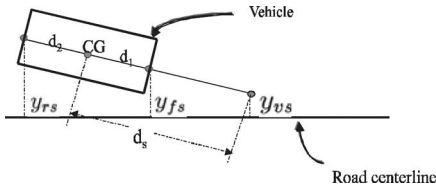


Fig. 10. Geometric look-ahead scheme.

then the LIDAR measurements may have a strong correlation with that of the magnetometers. However, such an assumption has never been verified before.

Currently, there are two sets of magnetometers installed on each PATH test vehicle, one under the front bumper and the other under the rear bumper. Fig. 9 shows the outputs of the two sets of magnetometers during the testing. It can be seen that the output from the front magnetometers has a phase lead over the output from the rear magnetometers. Such a phase lead may be further increased by using a geometric look-ahead scheme as shown in Fig. 10, as the outputs of the front and rear magnetometers are incorporated to calculate the vehicle's virtual lateral deviation measured at distance d_s ahead of the vehicle center of gravity (CG) according to

$$y_{vs} = \frac{(d_2 + d_s)y_{fs} + (d_1 - d_s)y_{rs}}{d_1 + d_2} \quad (46)$$

where y_{fs} and y_{rs} are the front and rear magnetometer outputs respectively, and d_1 and d_2 denote the distances from the front and rear magnetometers to the vehicle CG. As shown in Fig. 11, the phase lead in the vehicle lateral dynamics increases with larger look-ahead distance. By extending this look-ahead scheme, one may reasonably expect that the lateral LIDAR measurement can be interpreted as the lateral deviation at a large look-ahead distance. In this case, the look-ahead distance also varies with the relative longitudinal intervehicle distance x_r . Hence, the approximated look-ahead lateral deviation becomes

$$y_{vs} = \frac{(d_2 + x_r)y_{fs} + (d_1 - x_r)y_{rs}}{d_1 + d_2}. \quad (47)$$

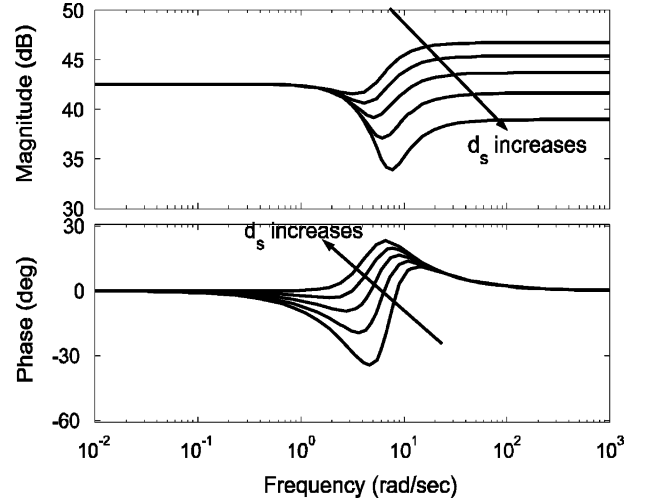


Fig. 11. Frequency response of the transfer function from front tire steering angle to lateral acceleration at look-ahead distance.

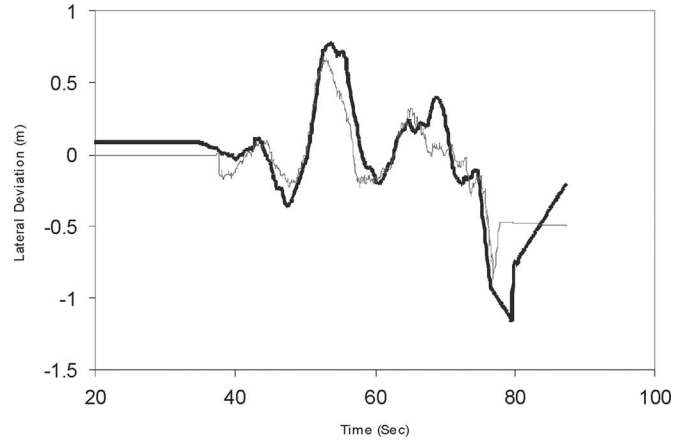


Fig. 12. Comparing the outputs from LIDAR and magnetometers. Look-ahead error generated from magnetometer measurements (*thin line*). Lateral measurement from LIDAR (*thick line*).

To investigate the relation between LIDAR and magnetometer measurements, the LIDAR sensor has to be accurately calibrated so that no bias exists in either distance or orientation measurement. The calibration of the orientation measurement is especially critical, as a very small bias in the orientation output may result in a large bias in lateral LIDAR measurements for a target at a large distance. Since this bias varies with longitudinal distance, it is hard to identify and compensate in either online or offline processing. Fig. 12 compares the LIDAR measurements to the look-ahead lateral deviation, as composed according to (47), from the two magnetometer outputs. It can be seen from this figure that LIDAR does provide as much phase lead as the deviation constructed by the look-ahead scheme in (47). In fact, the phase lead provided by LIDAR is larger than the one generated by the look-ahead scheme. This is due to the fact that as the look-ahead distance increases, the road curvature starts to have more effects which cannot be predicted by the magnetometer measurements. For the same reason, the LIDAR outputs are seen to be generally larger than that of the look-ahead deviation in

terms of the magnitude. The tracking performance of the lead vehicle also affects the LIDAR measurements, and in all the experiments, the maximum lateral error of the lead vehicle was maintained at less than 10 cm.

Hence, from the experimental results, one may reasonably consider LIDAR lateral output as lateral deviation of the vehicle measured at the look-ahead distance x_r , in terms of the phase lead it provides. This makes it possible to construct a vehicle lateral guidance system solely based on LIDAR measurements, i.e., AVF control. As the vehicle is controlled to follow another vehicle based on the LIDAR measurements, no other sensors, e.g., magnetometers, and road infrastructure are necessary. Within the magnetic reference scheme, LIDAR may also be used to compensate the magnetometer measurements when some of these magnetometers fail. Especially, as revealed by previous research [15], [16], the failure of the front magnetometers places significant challenges to the controller design due to the lack of phase lead in the vehicle lateral dynamics. In this case, the loss of phase lead may be compensated by the use of the LIDAR sensor.

VII. CONCLUSION

This paper has described a new sensor, i.e., the LIDAR sensor, for the California PATH vehicle lateral guidance system. It has also introduced the working scheme of this LIDAR sensor, and presented the data processing algorithm used for the LIDAR measurements. The proposed probabilistic data association based algorithm has been verified in real-time experiments using two Buick test vehicles. The testing results show that the estimated relative intervehicle speed matches the recorded wheel speed, suggesting that the sensor was successfully tracking the lead vehicle. The experimental study has also revealed the relation between LIDAR outputs and magnetometer measurements, as it shows that the LIDAR output may be roughly approximated by the look-ahead scheme using the outputs from the two sets of magnetometers. This demonstrates that LIDAR may be reasonably considered as a look-ahead sensor, which provides considerable amount of phase lead. Such a discovery can be used to develop a new lateral control system that is based on LIDAR as the only sensor, i.e., AVF control, or a sensor management/fusion system combining the LIDAR sensor with the current magnetometers. The measurement redundancy contained in the fusion system allows the future development of fault-detection and fault-tolerant systems for enhanced safety in the lateral guidance system.

REFERENCES

- [1] J. K. Hedrick, M. Tomizuka, and P. Varaiya, "Control issues in automated highway systems," *IEEE Control Syst. Mag.*, vol. 14, no. 6, pp. 21–32, Dec. 1994.
- [2] P. Varaiya, "Smart carts on smart roads: Problems of control," *IEEE Trans. Autom. Control*, vol. 38, no. 2, pp. 195–207, Feb. 1993.
- [3] C. Chen, "Backstepping design of nonlinear control systems and its application to vehicle lateral control in automated highway systems" Ph.D. dissertation, Univ. California, Berkeley, 1996.
- [4] P. Hingwe and M. Tomizuka, "Robust and gain scheduled H_∞ controllers for lateral guidance of passenger vehicles in AHS," in *Proc. ASME Dynam. Syst. Control Division*, 1997, vol. 61, Nov. 1997, pp. 707–713.

- [5] J.-Y. Wang and M. Tomizuka, "Dynamics analysis and robust steering controller design for automated lane guidance of heavy-duty vehicles," *Asian J. Control*, vol. 2, no. 3, pp. 140–154, Sep. 2000.
- [6] M. Bertozzi and A. Broggi, "Vision-based vehicle guidance," *Computer*, vol. 30, no. 7, pp. 49–55, Jul. 1997.
- [7] J. Goldbeck, B. Huertgen, S. Ernst, and L. Kelch, "Lane following combining vision and DGPS," *Image Vis. Comput.*, vol. 18, pp. 425–433, 2000.
- [8] J. Kosecha, R. Blasi, C. J. Taylor, and J. Malik, "Vision-based lateral control of vehicles," in *Proc. IEEE Conf. Intell. Transp. Syst.*, New York, Nov. 9–12, 1997, pp. 900–905.
- [9] K. A. Redmill, "A simple vision system for lane keeping," in *Proc. IEEE Conf. Intell. Transp. Syst.*, New York, Nov. 9–12, 1997, pp. 212–217.
- [10] T. Fujioka and M. Omae, "Vehicle following control in lateral direction for platooning," *Vehicle Syst. Dynam. Suppl.*, vol. 28, pp. 422–437, 1998.
- [11] S. Gehrig and F. Stein, "A trajectory-based approach for the lateral control of car following systems," in *Proc. IEEE Int. Conf. Intell. Vehicles*, vol. 4, Oct. 11–14, 1998, pp. 3596–3601.
- [12] G. Lu and M. Tomizuka, "A laser scanning radar based autonomous lateral vehicle following control scheme for automated highways," in *Proc. 2003 Am. Control Conf.*, Denver, CO, Jun. 4–6, 2003, pp. 30–35.
- [13] Y. Bar-Shalom and E. Tse, "Tracking in a cluttered environment with probabilistic data association," *Automatica*, vol. 11, pp. 451–460, 1975.
- [14] X. R. Li and Y. Bar Shalom, "Design of an interacting multiple model algorithm for air traffic control tracking," *IEEE Trans. Control Syst. Technol.*, vol. 1, no. 3, pp. 186–194, Sep. 1993.
- [15] J. Huang, G. Lu, and M. Tomizuka, "Vehicle lateral control under fault in front and/or rear sensors," Univ. California Berkeley, *California PATH Res. Rep. UCB-ITS-PRR-2000-25*, 2000.
- [16] S. Patwardhan, H.-S. Tan, and J. Guldner, "A general framework for automatic steering control: System analysis," in *Proc. 1997 Am. Control Conf.*, 1997, pp. 1598–1602.



Guang Lu (M'04) received the B.E. degree in precision instruments and machinery from Tsinghua University, Beijing, China, in 1997, the M.S. degree in mechanical engineering from the University of Alabama, Tuscaloosa, in 1999, and the Ph.D. degree in mechanical engineering from the University of California, Berkeley, in 2004.

Since July 2004, he has been an Assistant Professor in the Department of Mechanical Engineering, Tulane University, New Orleans, LA. His current research interests include vehicle control, system theory, intelligent sensors, and precision control.



Masayoshi Tomizuka (M'86–SM'95–F'97) was born in Tokyo, Japan, in 1946. He received the B.S. and M.S. degrees from Keio University, Tokyo, Japan, in 1968 and 1970, respectively, and the Ph.D. degree from the Massachusetts Institute of Technology, Cambridge, in 1974, all in mechanical engineering.

In 1974, he joined the faculty of the Department of Mechanical Engineering, University of California, Berkeley, where he currently holds the Cheryl and John Neerhout, Jr., Distinguished Professorship Chair. At the University of California, his teaching interests include dynamic systems and controls. His current research interests include optimal and adaptive control, digital control, signal processing, motion control, and control problems related to robotics, machining, manufacturing, information storage devices, and vehicles. He was a Consultant to various organizations, including the Lawrence Berkeley Laboratory, General Electric, General Motors, and United Technologies.

Dr. Tomizuka is a Fellow of the American Society of Mechanical Engineers (ASME) and the Society of Manufacturing Engineers. He is the recipient of the J-DSMC Best Paper Award in 1995, the ASME's Dynamic Systems and Control Division (DSCD) Outstanding Investigator Award in 1996, the Charles Russ Richards Memorial Award in 1997, and the Rufus Oldenburger Medal in 2002. He was a Technical Editor of the *ASME Journal of Dynamic Systems, Measurement and Control* (J-DSMC) from 1988 to 1993, the Editor-in-Chief of the IEEE/ASME TRANSACTIONS ON MECHATRONICS from 1997 to 1999, and an Associate Editor of the *Journal of the International Federation of Automatic Control, Automatica*, and the *European Journal of Control*. He was the General Chairman of the 1995 American Control Conference, and the President of the American Automatic Control Council from 1998 to 1999.